Organic Electronics xxx (2015) xxx–xxx

Contents lists available at ScienceDirect

Organic Electronics

journal homepage: www.elsevier.com/locate/orgel

A low bandgap carbazole based small molecule for organic solar cells

Miaomiao Li, Wang Ni, Huanran Feng, Xiangjian Wan, Yongtao Liu, Yi Zuo, Bin Kan, Qian Zhang, Yongsheng Chen *

State Key Laboratory and Institute of Elemento-Organic Chemistry, Centre for Nanoscale Science and Technology, Institute of Polymer Chemistry, College of Chemistry, Nankai University, Tianjin 300071, China
Collaborative Innovation Center of Chemical Science and Engineering (Tianjin), Nankai University, Tianjin 300071, China

ARTICLE INFO

Article history:
Received 4 April 2015
Received in revised form 11 May 2015
Accepted 16 May 2015
Available online xxxx

Keywords:
Organic solar cell
Small molecule
Solution processed
Low bandgap
Thiobarbituric acid

ABSTRACT

A new A–D–A small molecule, named **DTB3TCz**, with a weak electron donating unit (carbazole) as the core and a strong electron withdrawing unit (thiobarbituric acid) as the terminal acceptor, was designed and synthesized for organic solar cells. The new molecule shows deep highest occupied molecular orbital (HOMO) and lowest unoccupied molecular orbital (LUMO) energy levels, and narrow optical band gap of 1.61 eV. The device based on **DTB3TCz**:$PC_{71}BM$ blend film without any post treatment shows a high open circuit voltage (V_{oc}) of 1.04 V and the optimized device shows a high short-circuit current density (J_{sc}) of 11.80 mA cm^{-2} and a power conversion efficiency of 5.26%.

1. Introduction

Solution processed organic photovoltaics (OPVs) are considered as a promising alternative to silicon-based photovoltaic because of their unique advantages of low cost, light-weight, and potential to fabricate flexible large-area devices [1–4]. Polymer-based OPVs have drawn a great amount of attention [5–10], and the power conversion efficiencies (PCEs) of over 10% for a single junction and over 11% for tandem junction organic solar cells have been achieved [11–18]. Meanwhile, small-molecule-based OPVs are emerging as a competitive alternative to their polymeric counterparts due to several important advantages of small molecules, such as high purity, well defined structure and molecular weight, and thus no batch-to-batch variations [19–22]. Recently, PCEs of ~10% have been achieved for small molecule based OPVs [23–26]. To further improve the PCE and achieve commercialization of OPVs, innovation of photoactive materials, especially for donor materials, is still an important and necessary approach for both polymer based OPVs and small molecule based OPVs.

PCE is determined by the three parameters including open-circuit voltage (V_{oc}), short-circuit current (J_{sc}), and fill factor (FF). Among these three parameters, V_{oc} and J_{sc} are highly depended on the energy level of donor materials. V_{oc} is tightly correlated with the energy level difference between the highest occupied molecular orbital (HOMO) of the donor material and the lowest unoccupied molecular orbital (LUMO) of the acceptor material for OPV devices [27–29]. Thus, high V_{oc} could be achieved through lowering the HOMO energy levels of the donor. For J_{sc}, light absorption of the donor materials is the most fundamental factor, which can be improved by lowering the band gap of the donors to extend the absorption to longer wavelengths. The band gap is determined by the difference of the HOMO energy level and the LUMO energy level of the donor material. Therefore, the donor molecule should have both deep LUMO and HOMO energy levels, in order to obtain high V_{oc} and J_{sc} simultaneously, thus high performance photovoltaic devices.

As one type of D–A structure small molecules, A–D–A molecules exhibit outstanding photovoltaic performance [30–36]. A–D–A small molecules generally consist of an electron-donating segment (D) as the core unit, two electron-accepting segments (A) as the terminal groups, and oligothiophenes as the π-conjugated bridges to link the central donor unit and the terminal acceptor units. For A–D–A small molecules, the HOMO energy levels are mainly decided by the central donor segments, and the LUMO energy levels are more related to the terminal acceptor segments [37,38]. Therefore, for OPVs based on A–D–A small donor molecules, high V_{oc} and J_{sc} could be achieved by the strategy of incorporating central donor units with weak electron donating ability and terminal acceptor units with strong electron withdrawing ability

* Corresponding author at: State Key Laboratory and Institute of Elemento-Organic Chemistry, Centre for Nanoscale Science and Technology, Institute of Polymer Chemistry, College of Chemistry, Nankai University, Tianjin 300071, China.
E-mail address: yschen99@nankai.edu.cn (Y. Chen).

http://dx.doi.org/10.1016/j.orgel.2015.05.024
1566-1199/

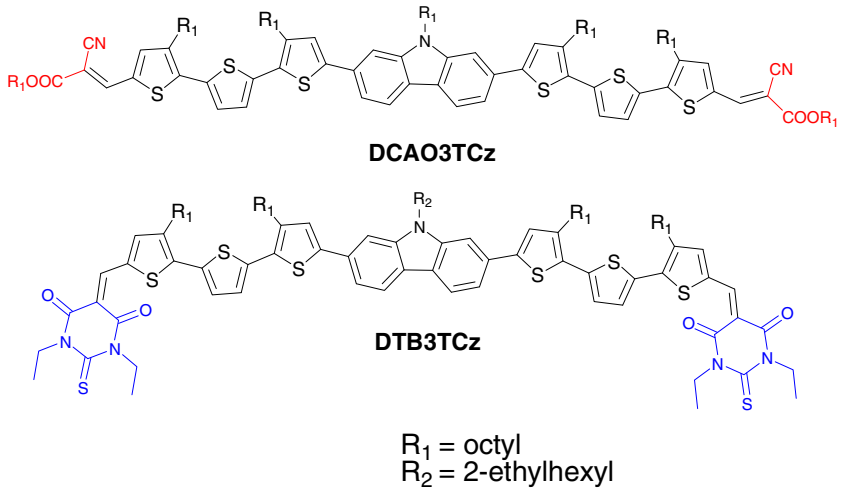

Fig. 1. Chemical structures of DCAO3TCz and **DTB3TCz**.

into the molecules to lower their HOMO and LUMO energy levels simultaneously. Carbazole, with weak electron donating ability, is one of the most important aromatic units for designing high-performance polymers/molecules for photovoltaic cells [39–45]. Recently, we have reported a A–D–A small molecule named **DCAO3TCz** with 2,7-carbazole as the core and alkyl cyanoacetate as the terminal (Fig. 1) [38]. The device based on **DCAO3TCz** showed high V_{oc} over 0.9 V due to the deep HOMO level (−5.14 eV), but relatively low J_{sc} with value of ~6 mA cm^{-2}, mainly attributed to the relatively large band gap (~1.90 eV).

Herein, based on our previous works, we designed and synthesized a new small molecule, named **DTB3TCz** (Fig. 1), consisting of the weak electron-donating carbazole as the central donor unit and strong electron-withdrawing thiobarbituric acid as the terminal acceptor. Thiobarbituric acid, as a high electron affinity unit, has been applied in OPV small molecules reported by several groups [46–48]. Through the replacement of alkyl cyanoacetate with thiobarbituric acid, **DTB3TCz** achieves reduced LUMO energy level and a much lower optical band gap of 1.61 eV. Besides, owing to its weak electron-donating ability of cabazole unit, the new molecule maintains deep HOMO energy level of −5.16 eV. The photovoltaic device based on **DTB3TCz**:$PC_{71}BM$ blend film without any post treatment yielded a high V_{oc} of 1.04 V. The optimized device showed a PCE of 5.26% with a much improved J_{sc} of 11.80 mA cm^{-2}, compared with the device based on **DCAO3TCz**. To our knowledge, it is the highest PCE for the carbazole based small molecule organic solar cells so far. These results suggest that designing A–D–A small molecules with the strategy of weak electron-donating units as central donors and strong electron-withdrawing units as terminal acceptors could be an efficient approach to obtain high V_{oc} and J_{sc} simultaneously.

2. Experiment

2.1. Materials and synthesis

All reactions and manipulations were carried under an argon atmosphere using standard Schlenk techniques. All starting materials were purchased from commercial suppliers and used without further purification. Compounds **1** and **2** were synthesized according to the literatures [23,41]. Synthesis of **DTB3TCz** is outline in Scheme 1.

Compound 3 (DTB3TCz). A solution of compounds **1** (0.90 g, 1.69 mmol) and **2** (2.2 g, 3.80 mmol) in toluene (45 mL) and

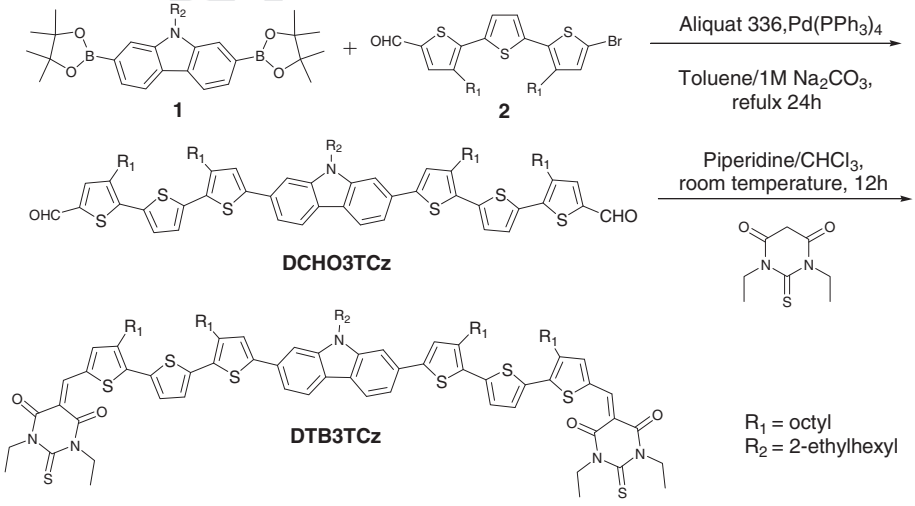

Scheme 1. Synthesis routes of **DTB3TCz**.

Please cite this article in press as: M. Li et al., A low bandgap carbazole based small molecule for organic solar cells, Org. Electron. (2015), http://dx.doi.org/10.1016/j.orgel.2015.05.024

aqueous 1 M Na_2CO_3 solution (15 mL) was degassed twice with argon, Then $Pd(PPh_3)_4$ (30 mg, 0.026 mmol) and Aliquat 336 (0.15 mL) was added and the mixture was stirred at 100 °C for 24 h under argon. The mixture was then poured into water (200 mL), and extracted with chloroform. The organic layer was washed with water, and then dried over anhydrous Na_2SO_4. The solvent was removed by a rotating evaporator and the residue was purified by silica gel chromatography using a mixture of petroleum ether and dichloromethane (1:1) as eluant to produce compound **3** (1.1 g, 50%).^{1}H NMR (400 MHz, $CDCl_3$): δ 9.83 (s, 2H), 8.03 (d, *J* = 7.6 Hz, 2H), 7.60 (s, 2H), 7.54 (s, 2H), 7.49 (d, *J* = 7.6 Hz, 2H), 7.27 (d, *J* = 4.0 Hz, 2H), 7.26 (s, 2H), 7.17 (d, *J* = 4.0 Hz, 2H), 4.20 (m, 2H), 2.85 (m, 8H), 2.11 (m, 1H), 1.73 (m, 8H), 1.30 (m, 48H), 0.89 (m, 18H). ^{13}C NMR (100 MHz, $CDCl_3$): δ 182.49, 143.84, 141.96, 141.40, 141.17, 140.25, 140.18, 139.06, 138.58, 134.31, 131.58, 129.15, 127.84, 126.20, 125.95, 122.35, 120.66, 117.38, 105.87, 77.35, 77.03, 76.71, 47.20, 39.49, 31.93, 31.89, 31.02, 30.65, 30.33, 29.82, 29.71, 29.52, 29.44, 29.33, 29.28, 28.94, 24.69, 23.10, 22.70, 14.21, 14.12, 11.05. MS (MALDI-TOF): calcd for $C_{78}H_{101}NO_2S_6$ [M^+], 1275.61; found: 1275.58.

Compound DTB3TCz. Compound **3** (0.30 g, 0.24 mmol) and thiobarbituric acid (0.5 g, 2.5 mmol) was dissolved in a solution of dry chloroform (60 mL), then three drops of piperidine were added, the mixture was stirred overnight under argon at room temperature. The solvent was then removed by a rotating evaporator and the crude product was dissolved in 10 mL of chloroform, then precipitated from methanol and the precipitate was filtered off. The residue was purified by silica gel chromatography using a mixture of petroleum ether and chloroform (2:1) as eluent and the crude solid was recrystallized from a hexane and chloroform mixture three times to produce **DTB3TCz** (0.28 g, 71%). ^{1}H NMR (400 MHz, $CDCl_3$): δ 8.53 (s, 2H), 8.01 (d, *J* = 7.6 Hz, 2H), 7.66 (s, 2H), 7.55–7.45 (m, 6H), 7.25 (s, 2H), 7.20 (d, *J* = 4.0 Hz, 2H), 4.58 (m, 8H), 4.17 (m, 2H), 2.84 (m, 8H), 2.09 (m, 1H), 1.72 (m, 8H), 1.43–1.28 (m, 60H), 0.99–0.83 (m, 18H). ^{13}C NMR (100 MHz, $CDCl_3$): δ178.64, 161.06, 159.88, 149.83, 148.96, 148.76, 144.09, 141.95, 141.69, 140.54, 140.15, 134.54, 134.27, 131.47, 129.23, 128.98, 126.31, 126.05, 122.40, 120.67, 117.32, 109.70, 105.82, 43.93, 43.12, 39.51, 31.93, 31.90, 31.04, 30.55, 29.99, 29.75, 29.60, 29.54, 29.48, 29.42, 29.36, 29.31, 28.99, 24.73, 23.11, 22.70, 14.24, 14.13, 12.55, 12.41, 11.08. MS (MALDI-TOF): calcd for $C_{94}H_{121}N_5O_4S_8$ [M^+], 1639.72; found: 1639.72. Anal. Calcd. for $C_{94}H_{121}N_5O_4S_8$: C, 68.78; H, 7.43; N, 4.27. Found: C, 68.61; H, 7.34; N, 4.38.

2.2. Measurements and instruments

The ^{1}H and ^{13}C nuclear magnetic resonance (NMR) spectra were taken on a Bruker AV400 Spectrometer. Matrix assisted laser desorption/ionization time-of-flight (MALDI-TOF) mass spectra were performed on a Bruker Autoflex III instrument. The thermogravimetric analyses (TGA) were carried out on a NETZSCH STA 409PC instrument under purified nitrogen gas flow with a 10 °C min^{-1} heating rate. UV–vis spectra were obtained with a JASCO V-570 spectrophotometer. Atomic force microscope (AFM) investigation was performed using Bruker MultiMode 8 in "tapping" mode. The transmission electron microscope (TEM) investigation was performed on a Philips Technical G2 F20 at 200 kV. Cyclic voltammetry (CV) experiments were performed with a LK98B II Microcomputer-based Electrochemical Analyzer in dichloromethane solutions. All CV measurements were carried out at room temperature with a conventional three-electrode configuration employing a glassy carbon electrode as the working electrode, a saturated calomel electrode (SCE) as the reference electrode, and a Pt wire as the counter electrode. Dichloromethane was distilled from calcium hydride under dry argon immediately prior to use. Tetrabutylammonium phosphorus hexafluoride (Bu_4NPF_6, 0.1 M) in dichloromethane was used as the supporting electrolyte, and the scan rate was 100 mV s^{-1}. Hole mobility was measured by space charge limited current (SCLC) method using a diode configuration of ITO/PEDOT:PSS/donor:$PC_{71}BM$/Au by taking the dark current density in the range of 0–6 V and fitting the results to a space charge limited form, where SCLC is described by:

$$J = \frac{9\varepsilon_0\varepsilon_r\mu_0 V^2}{8L^3}\exp\left(0.89\beta\sqrt{\frac{V}{L}}\right)$$

where *J* is the current density, *L* is the film thickness of the active layer, μ_0 is the hole mobility, ε_r is the relative dielectric constant of the transport medium, ε_0 is the permittivity of free space (8.85×10^{-12} F m^{-1}), *V* (=$V_{appl} - V_{bi}$) is the internal voltage of the device, V_{appl} is the applied voltage to the device and V_{bi} is the built-in voltage due to the relative work function difference of the two electrodes.

The current density–voltage (*J*–*V*) characteristics of photovoltaic devices were obtained by a Keithley 2400 source-measure unit. The photocurrent was measured under illumination simulated 100 mW cm^{-2} AM1.5G irradiation using a xenon-lamp-based solar simulator [Oriel 96000 (AM1.5G)] in an argon filled glove box. Simulator irradiance was characterized using a calibrated spectrometer and illumination intensity was set using a certified silicon diode. External quantum efficiency (EQE) value of the encapsulated device was obtained with a halogen-tungsten lamp, monochromator, optical chopper, and lock-in amplifier in air and photon flux was determined by a calibrated silicon photodiode.

2.3. Fabrication of organic solar cells

The photovoltaic devices were fabricated with a structure of glass/ITO/PEDOT:PSS/donor:acceptor/ETL-1 or ZnO/Al. ETL-1 used as the interfacial layer for cathodes is a methanol-soluble fullerene-surfactant developed by Alex [49], and its structure is shown as Fig. S1. The ITO-coated glass substrates were cleaned subsequently by ultrasonic treatment in detergent, deionized water, acetone, and isopropyl alcohol under ultrasonication for 15 min each solvent and then dried by a nitrogen flow. A thin layer of PEDOT:PSS (Baytron P VP AI 4083, filtered at 0.45 μm) was spin-coated (3000 rpm, ca. 40 nm thick) onto ITO surface. After being baked at 150 °C for 20 min, the substrates were transferred into an argon-filled glove box. Then, the active layer was spin-coated from **DTB3TCz** (10 mg/mL):[6,6]-phenyl-C_{71}-butyric acid methyl ester ($PC_{71}BM$) blend chloroform solution with different ratios at 1700 rpm for 20 s. Subsequently, ETL-1 solution (0.5 mg/mL, dissolved in methanol) or ZnO particle suspension was spin-coated at 3000 rpm. Finally, 50 nm Al layer was deposited on ETL-1 film under high vacuum (<2×10^{-4} Pa). Thermal annealing was carried out on a digitally controlled hotplate at various temperatures after Al layer deposition in an argon-filled glove box. The thickness of active layer was measured using Dektak 150 profilometer. The effective area of each cell was 4 mm^2 defined by masks for the solar cell devices discussed in this work.

3. Results and discussion

3.1. Synthesis and thermal property

The synthesis of **DTB3TCz** is outlined in Scheme 1. The intermediates of dialdehyde compound **3** was synthesized from Suzuki coupling in refluxing toluene for 24 h, using Na_2CO_3 as the base under an argon atmosphere in the presence of Aliquat336 and $Pd(PPh_3)_4$ as the catalyst. The target molecule, **DTB3TCz** was then

Please cite this article in press as: M. Li et al., A low bandgap carbazole based small molecule for organic solar cells, Org. Electron. (2015), http://dx.doi.org/10.1016/j.orgel.2015.05.024

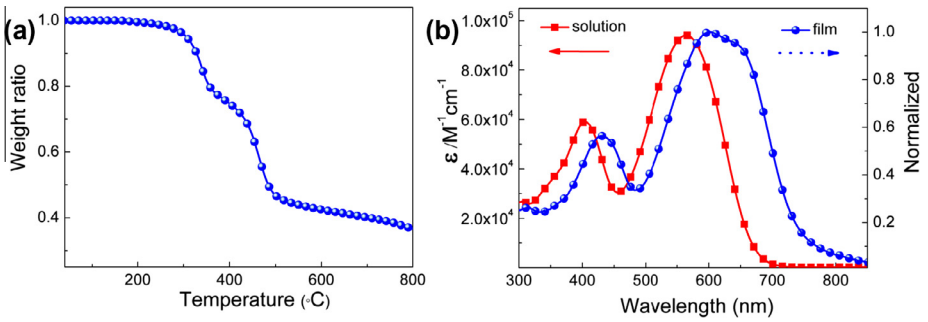

Fig. 2. (a) TGA curve of **DTB3TCz** with a heating rate of 10 °C/min under N_2 atmosphere; (b) absorption spectra of **DTB3TCz** in chloroform solution and in an as-cast film.

prepared by Knoevenagel condensation of **DCHO3TCz** with thiobarbituric acid. This new molecule exhibits good thermal stability up to 300 °C under N_2 atmosphere (Fig. 2a).

3.2. Optical properties

The UV–Vis absorption spectra of **DTB3TCz** in diluted chloroform and in the thin solid state are showed in Fig. 2b. The detailed absorption data, including the absorption maxima in solution and film as well as the optical band gap, are summarized in Table 1. As shown in Fig. 2b, **DTB3TCz** in chloroform solution shows an absorption peak at 564 nm with a maximum absorption coefficient of 9.4×10^4 M^{-1} cm^{-1}. The **DTB3TCz** film cast from the chloroform solution shows a broader absorption and a red-shifted absorption peak at 600 nm. In addition, the absorption of the film exhibits a full coverage from 300 to 770 nm, indicating the high light harvesting ability of the molecule. The optical band gap of **DTB3TCz** is estimated to be 1.61 eV from the onset of the film absorption spectrum. The optical band gap of **DTB3TCz** is much lower than that of molecule **DCAO3TCz** (1.92 eV) with alkyl cyanoacetate group as the acceptor [38]. The absorption results demonstrate that the introducing of thiobarbituric acid, as terminal acceptor unit could efficiently reduce the optical band gap of carbazole based A–D–A small molecules.

3.3. Electrochemical properties

The electrochemical properties of **DTB3TCz** were investigated using a cyclic voltammogram and the data are summarized in Table 1. As shown in Fig. 3, the HOMO and LUMO energy levels at −5.16 and −3.56 eV respectively, are calculated from the onset oxidation and reduction potential of the redox curves. Compared with **DCAO3TCz** with HOMO/LUMO levels of −5.14/−3.21 eV [38], **DTB3TCz** exhibits similar HOMO level, but much deeper LUMO level. The electrochemical band gap of **DTB3TCz** is estimated to be 1.60 eV, which is consistent with the optical band gap. The deep HOMO energy level and low band gap could be beneficial for obtaining high V_{oc} and J_{sc} (Table 2).

3.4. Photovoltaic properties

Organic solar cells were fabricated using **DTB3TCz** as the electron donor with a general device structure of indium tin oxide (ITO)/PEDOT:PSS/DTB3TCz:PC_{71}BM/ETL-1/Al using the conventional solution spin-coating process. Device optimization was conducted by varying the weight ratios of donor *vs.* acceptor (summarized in Table S1). The best result was observed for a donor/acceptor weight ratio of 1:0.8 from chloroform solution with a donor concentration of 10 mg mL^{-1}. As shown in Fig. 4a, the device with the blend of **DTB3TCz** and PC_{71}BM gave a high V_{oc} of 1.04 V, a J_{sc} of 5.37 mA cm^{-2}, a *FF* of 0.29 and a PCE of 1.62%. The impressively high V_{oc} demonstrates that molecules with weak donor unit carbazole as central block unit could provide high V_{oc} for photovoltaic devices. Further improvement of the PCE was achieved by gradient heating process after the device fabricated.

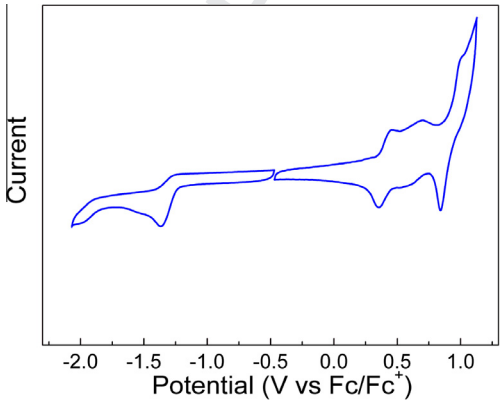

Fig. 3. Cyclic voltammogram of **DTB3TCz** in a dichloromethane solution of 0.1 mol L^{-1} Bu_4NPF_6 with a scan rate of 100 mV s^{-1}.

Table 2
Photovoltaic performance of organic photovoltaic devices based on **DTB3TCz**:PC_{71}BM blend films with weight ratios (w:w) of 1:0.8, under an illumination of AM 1.5 G, 100 mW cm^{-2}.

Treatment	V_{oc} (V)	J_{sc} (mA cm^{-2})	*FF* (%)	PCE_{max} (PCE_{ave}[a])
No annealing [b]	1.04	5.37	0.29	1.62% (1.50%)
120 °C TA [b]	0.91	11.80	0.49	5.26% (5.02%)
120 °C TA [c]	0.92	11.63	0.47	5.03% (4.89%)

[a] The average PCE is obtained from 20 devices.
[b] ETL-1 as electron transport layer.
[c] ZnO as electron transport layer.

Table 1
Optical and electrochemical data of **DTB3TCz**.

Compound	λ_{max} solution /nm	ε solution /$M^{-1}cm^{-1}$	λ_{max} film /nm	E_g^{opt} film /eV	E_g^{CV} /eV	HOMO /eV	LUMO /eV
[a]DCAO3TCz	485	8.3×10^4	536	1.92	1.93	−5.14	−3.21
DTB3TCz	564	9.4×10^4	600	1.61	1.60	−5.16	−3.56

[a] Data from Ref. [38].

Please cite this article in press as: M. Li et al., A low bandgap carbazole based small molecule for organic solar cells, Org. Electron. (2015), http://dx.doi.org/10.1016/j.orgel.2015.05.024

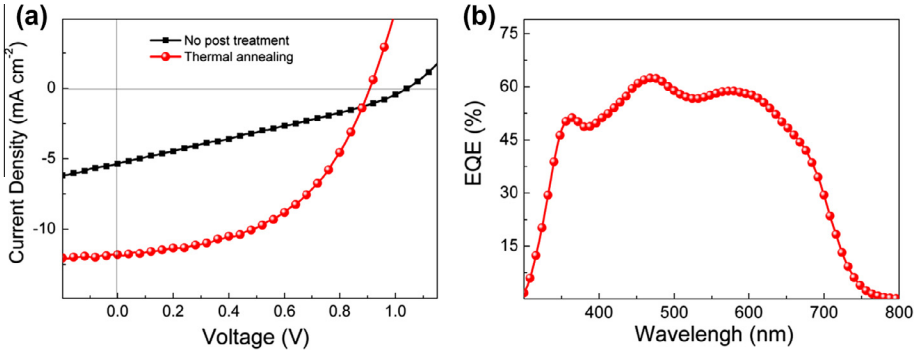

Fig. 4. (a) Characteristic current density versus voltage (*J*–*V*) curves of **DTB3TCz**:$PC_{71}BM$ (1:0.8, w/w) without post treatment and with thermal annealing at 120 °C for 10 min; (b) EQE of the device based on **DTB3TCz**:$PC_{71}BM$ (1:0.8, w/w) after thermal annealing at 120 °C for 10 min.

The results of thermal annealing treatment are shown in Table S2. After 120 °C thermal annealing treatment, the device exhibited the highest PCE of 5.26% with a V_{oc} of 0.91V, a J_{sc} of 11.80 mA cm^{-2} and a FF of 0.49. The increased J_{sc} and FF could be due to the improved morphology, as discussed below. The decreased V_{oc} of the device with thermal annealing treatment could be attributed to the increasing intermolecular interaction between the donor and acceptor, which has been observed in our previous works [50]. The intermolecular interaction (or electronic coupling) between the donor and acceptor has great influence on the V_{oc} and improving the intermolecular interaction between the donor and acceptor would increase the J_{sc} and decrease the V_{oc} [50,51]. Thermal annealing could improve the intermolecular interaction between the donor and acceptor in the **DTB3TCz**:$PC_{71}BM$ blend film, resulting in the decreased V_{oc}. Furthermore, for comparison with the device based on DCAO3TCz using ZnO as interfacial layer, the **DTB3TCz**-based devices with ZnO was fabricated, and showed a PCE of 5.03%, which is much higher than that of DCAO3TCz (3.63%). The high performance of **DTB3TCz** is mainly attributed to the increased J_{sc} (11.63 mA cm^{-2} for **DTB3TCz** and 6.15 mA cm^{-2} for DCAO3TCz) [38], indicating that introduction of strong electron-withdrawing acceptor block is an efficient way to improve J_{sc} and thus PCE. The external quantum efficiency (EQE) curve of the **DTB3TCz**-based device with 120 °C thermal annealing is shown in Fig. 4b. From the EQE spectrum, the **DTB3TCz**-based device exhibits very broad photo-to-current response from 300 to about 770 nm with the highest EQE value of about 63%. And owing to the narrow band gap, the photo-to-current response range of **DTB3TCz** is much broader than that of **DCAO3TCz** (from 300 to 650 nm). For the **DTB3TCz**-based device, the calculated J_{sc} obtained by integration of the EQE curve is 11.5 mA cm^{-2}, which shows a 2.5% mismatch compared with the J_{sc} value obtained from the *J*–*V* curve.

To further understand the photovoltaic performance of **DTB3TCz**-based devices, the photocurrent behavior of optimized devices was explored and the relationship of the photocurrent (J_{ph}) and effective voltage (V_{eff}) for the device with 120 °C thermal annealing is shown in Fig. 5. $J_{ph} = J_L - J_D$, where J_L and J_D are the current density under illumination and in the dark, respectively, V_{eff} is determined by the equation $V_{eff} = V_0 - V_a$, where V_a is the applied voltage, and V_0 is the voltage at which $J_{ph} = 0$ [52,53]. From Fig. 5a, the J_{ph} increase sharply with V_{eff} in lower voltage, and reaches gradually a saturated value (where saturation current density J_{sat} is obtained) in higher V_{eff}. The J_{sat} is generally correlated to the maximum exciton generation rate (G_{max}), which is a measure of the maximum number of photons absorbed [54]. The device exhibited a high J_{sat} up to 13.5 mA cm^{-2}, attributed to the broad absorption band and low band gap of **DTB3TCz**. The ratio of J_{ph}/J_{sat} can be used to judge the overall exciton dissociation

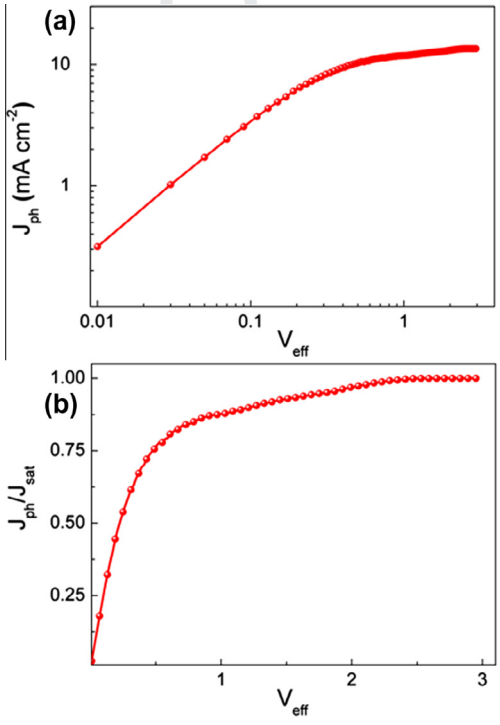

Fig. 5. (a) Photocurrent density and (b) charge collection efficiency versus effective voltage characteristics of the device with 120 °C thermal annealing under constant incident light intensity (AM 1.5G, 100 mW cm^{-2}).

efficiency and charge collection efficiency [55]. Fig. 5b plotted the normalized photocurrent (J_{ph}/J_{sat}) in the device with annealing 120 °C. The values of J_{ph}/J_{sat} are 87% and 66% under the short circuit and the maximal power output conditions, respectively. These demonstrate that the device has relatively low exciton dissociation efficiency and charge collection efficiency with much geminate or bimolecular recombination, compared with the high-performance organic photovoltaic devices [56] (up to 95% and 80% under the short circuit and the maximal power output conditions, respectively). Therefore, the OPV device based on **DTB3TCz** obtains the relatively low FF and the moderate EQE response.

3.5. Mobility and morphology

The hole mobilities of the **DTB3TCz**:$PC_{71}BM$ blend films through the hole-only device measured using the space charge limited current (SCLC) method are 2.56×10^{-5} cm^2 V^{-1} s^{-1} and 1.96×10^{-4} cm^2 V^{-1} s^{-1} for blend films without and with thermal

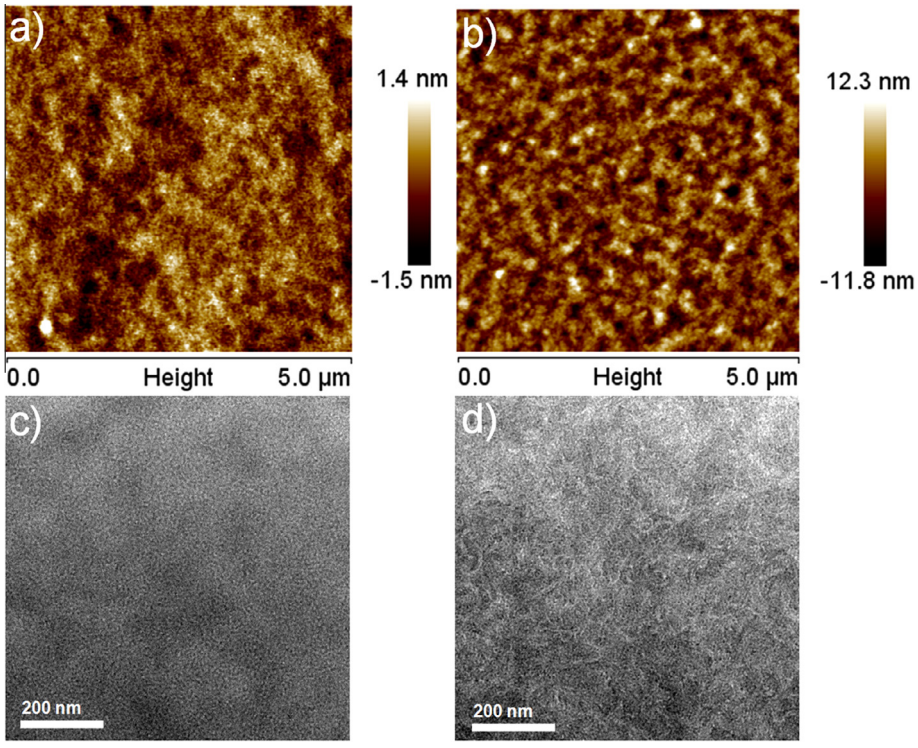

Fig. 6. (a and b) Tapping-mode AFM height images of the active layers of **DTB3TCz**:$PC_{71}BM$ (1:0.8, w/w). (a) Without annealing; (b) after thermal annealing at 120 °C for 10 min, (c and d) TEM images of **DTB3TCz** (1:0.8, w/w) blend film from $CHCl_3$. (c) Without annealing; (d) after annealing at 120 °C for 10 min.

annealing treatment, respectively (as plotted in Fig. S2). The hole mobility of DTB3TCz:$PC_{71}BM$ blend film with thermal annealing treatment is an order of magnitude higher than that of the film without any post treatment. The high mobility could be benefit for charge transport, thus leading to higher J_{sc}.

The morphologies of **DTB3TCz**:$PC_{71}BM$ blend films with different treatments were investigated by AFM and TEM. As shown in Fig. 6, root mean square (*rms*) roughness values are 0.33 and 2.74 nm for the blend films without post treatment and with thermal annealing, respectively. The low roughness values reveal that the films are smooth with high quality. The TEM images (Fig. 6) clearly show the differences between the morphologies of the blend films without and with thermal annealing. The film without any post-treatment shows no obvious phase separation of the donor and acceptor. After thermal treatment, the morphology exhibits obvious phase separation, and fiber-like domains with size of 20–30 nm are observed, which is comparable to the exciton diffusion length [57–59]. The better morphology benefits the exciton diffusion and dissociation, and charge transport, and reduces charge carriers recombination, thus improving J_{sc} and *FF*. However, the morphology of **DTB3TCz**:$PC_{71}BM$ blend film with thermal annealing is not fully optimized due to the unevenly distributed domains and some large aggregations, which are unfavor of exciton diffusion. Thus, the device shows the relatively low exciton dissociation efficiency and charge collection efficiency.

4. Conclusions

In this work, a new A–D–A small molecule **DTB3TCz**, based on the strategy of weak central donor unit and strong terminal acceptor unit, was designed and synthesized. The new molecule is comprised of the weak electron-donating unit, carbazole as the core, strong electron-withdrawing unit, thiobarbituric acid as the terminal acceptor, and terthiophene as the π-conjugated bridge. As expected, **DTB3TCz** exhibits deep HOMO/LUMO energy levels of −5.16/−3.56 eV, and low optical bandgap of 1.60 eV. The device based on **DTB3TCz**:$PC_{71}BM$ without any post treatment exhibits a high V_{oc} of 1.04 V, attributed to the deep HOMO level. After thermal annealing, the device of **DTB3TCz**:$PC_{71}BM$ showed a relatively high J_{sc} of 11.80 mA cm^{-2}, and a PCE of 5.26% which is the highest value for carbazole based small molecule organic solar cells. It is believed that there is still great potential for devices based on **DTB3TCz** to achieve higher PCEs through controlling and optimizing the morphology of active layer. More importantly, the results demonstrate that the strategy of weak central donor unit and strong electron withdrawing terminal acceptor could obtain both deep HOMO energy level and low optical band gap, and thus high V_{oc} and J_{sc} in small molecule organic solar cells.

Acknowledgments

The authors gratefully acknowledge the financial support from MOST (2014CB643502), NSFC (91433101, 51373078 and 51422304).

Appendix A. Supplementary data

Supplementary data associated with this article can be found, in the online version, at http://dx.doi.org/10.1016/j.orgel.2015.05.024.

References

[1] A.J. Heeger, Chem. Soc. Rev. 39 (2010) 2354–2371.
[2] A.C. Arias, J.D. MacKenzie, I. McCulloch, J. Rivnay, A. Salleo, Chem. Rev. 110 (2010) 3–24.
[3] F.C. Krebs, Sol. Energy Mater. Sol. Cells 93 (2009) 394–412.
[4] G. Dennler, M.C. Scharber, C.J. Brabec, Adv. Mater. 21 (2009) 1323–1338.
[5] L. Ye, S. Zhang, L. Huo, M. Zhang, J. Hou, Acc. Chem. Res. 47 (2014) 1595–1603.
[6] Y. Liang, L. Yu, Acc. Chem. Res. 43 (2010) 1227–1236.
[7] H. Zhou, L. Yang, A.C. Stuart, S.C. Price, S. Liu, W. You, Angew. Chem. Int. Ed. 50 (2011) 2995–2998.

[8] W. Li, W.S.C. Roelofs, M. Turbiez, M.M. Wienk, R.A.J. Janssen, Adv. Mater. 26 (2014) 3304–3309.
[9] P.M. Beaujuge, W. Pisula, H.N. Tsao, S. Ellinger, K. Müllen, J.R. Reynolds, J. Am. Chem. Soc. 131 (2009) 7514–7515.
[10] Y. Li, Acc. Chem. Res. 45 (2012) 723–733.
[11] J.-D. Chen, C. Cui, Y.-Q. Li, L. Zhou, Q.-D. Ou, C. Li, Y. Li, J.-X. Tang, Adv. Mater. 27 (2015) 1035–1041.
[12] Y. Liu, J. Zhao, Z. Li, C. Mu, W. Ma, H. Hu, K. Jiang, H. Lin, H. Ade, H. Yan, Nat. Commun. 5 (2014) 6293.
[13] S.-H. Liao, H.-J. Jhuo, P.-N. Yeh, Y.-S. Cheng, Y.-L. Li, Y.-H. Lee, S. Sharma, S.-A. Chen, Sci. Rep. 4 (2014) 06813.
[14] Z. He, B. Xiao, F. Liu, H. Wu, Y. Yang, S. Xiao, C. Wang, T.P. Russell, Y. Cao, Single-junction polymer solar cells with high efficiency and photovoltage, Nat. Photon 9 (2015) 174–179.
[15] C.-C. Chen, W.-H. Chang, K. Yoshimura, K. Ohya, J. You, J. Gao, Z. Hong, Y. Yang, Adv. Mater. 26 (2014) 5670–5677.
[16] A.R.B. Mohd Yusoff, D. Kim, H.P. Kim, F.K. Shneider, W.J. da Silva, J. Jang, Energy Environ. Sci. 8 (2015) 303–316.
[17] S. Zhang, L. Ye, W. Zhao, B. Yang, Q. Wang, J. Hou, Sci. China Chem. 58 (2015) 248–256.
[18] C. Liu, C. Yi, K. Wang, Y. Yang, R.S. Bhatta, M. Tsige, S. Xiao, X. Gong, A.C.S. App, Mater. Inter. 7 (2015) 4928–4935.
[19] J. Roncali, Acc. Chem. Res. 42 (2009) 1719–1730.
[20] J.E. Coughlin, Z.B. Henson, G.C. Welch, G.C. Bazan, Acc. Chem. Res. 47 (2013) 257–270.
[21] A. Mishra, P. Bäuerle, Angew. Chem. Int. Ed. 51 (2012) 2020–2067.
[22] G.W.P. Van Pruissen, F. Gholamrezaie, M.M. Wienk, R.A.J. Janssen, J. Mater. Chem. 22 (2012) 20387–20393.
[23] B. Kan, Q. Zhang, M. Li, X. Wan, W. Ni, G. Long, Y. Wang, X. Yang, H. Feng, Y. Chen, J. Am. Chem. Soc. 136 (2014) 15529–15532.
[24] V. Gupta, A.K.K. Kyaw, D.H. Wang, S. Chand, G.C. Bazan, A.J. Heeger, Sci. Rep. 3 (2013) 01965.
[25] K. Sun, Z. Xiao, S. Lu, W. Zajaczkowski, W. Pisula, E. Hanssen, J.M. White, R.M. Williamson, J. Subbiah, J. Ouyang, A.B. Holmes, W.W.H. Wong, D.J. Jones, Nat. Commun. 6 (2015) 7013.
[26] B. Kan, M. Li, Q. Zhang, F. Liu, X. Wan, Y. Wang, W. Ni, G. Long, X. Yang, H. Feng, Y. Zuo, M. Zhang, F. Huang, Y. Cao, T.P. Russell, Y. Chen, J. Am. Chem. Soc. 137 (2015) 3886–3893.
[27] H. Zhou, L. Yang, W. You, Macromolecules 45 (2012) 607–632.
[28] M.C. Scharber, D. Mühlbacher, M. Koppe, P. Denk, C. Waldauf, A.J. Heeger, C.J. Brabec, Adv. Mater. 18 (2006) 789–794.
[29] S.C. Price, A.C. Stuart, L. Yang, H. Zhou, W. You, J. Am. Chem. Soc. 133 (2011) 4625–4631.
[30] Z. Du, W. Chen, Y. Chen, S. Qiao, X. Bao, S. Wen, M. Sun, L. Han, R. Yang, J. Mater. Chem. A 2 (2014) 15904–15911.
[31] Y. Liu, C.-C. Chen, Z. Hong, J. Gao, Y. Yang, H. Zhou, L. Dou, G. Li, Sci. Rep. 3 (2013) 03356.
[32] Y. Lin, L. Ma, Y. Li, Y. Liu, D. Zhu, X. Zhan, Adv. Energy Mater. 4 (2014) 1300626.
[33] D. Deng, Y. Zhang, L. Yuan, C. He, K. Lu, Z. Wei, Adv. Energy Mater. (2014) 1400538.
[34] C.D. Wessendorf, G.L. Schulz, A. Mishra, P. Kar, I. Ata, M. Weidelener, M. Urdanpilleta, J. Hanisch, E. Mena-Osteritz, M. Lindén, E. Ahlswede, P. Bäuerle, Adv. Energy Mater. 4 (2014) 1400366.
[35] J. Min, Z.-G. Zhang, S. Zhang, Y. Li, Chem. Mater. 24 (2012) 3247–3254.
[36] Y. Zuo, Q. Zhang, X. Wan, M. Li, H. Zhang, C. Li, Y. Chen, Org. Electron. 19 (2015) 98–104.
[37] G. He, Z. Li, X. Wan, Y. Liu, J. Zhou, G. Long, M. Zhang, Y. Chen, J. Mater. Chem. 22 (2012) 9173–9180.
[38] W. Ni, M. Li, B. Kan, Y. Zuo, Q. Zhang, G. Long, H. Feng, X. Wan, Y. Chen, Org. Electron. 15 (2014) 2285–2294.
[39] S.H. Park, A. Roy, S. Beaupre, S. Cho, N. Coates, J.S. Moon, D. Moses, M. Leclerc, K. Lee, A.J. Heeger, Nat. Photon 3 (2009) 297–302.
[40] J. Li, A.C. Grimsdale, Chem. Soc. Rev. 39 (2010) 2399–2410.
[41] N. Blouin, A. Michaud, D. Gendron, S. Wakim, E. Blair, R. Neagu-Plesu, M. Belletête, G. Durocher, Y. Tao, M. Leclerc, J. Am. Chem. Soc. 130 (2007) 732–742.
[42] P. Li, H. Tong, J. Liu, J. Ding, Z. Xie, L. Wang, RSC Adv. 3 (2013) 23098–23104.
[43] P. Li, H. Tong, J. Ding, Z. Xie, L. Wang, J. Mater. Chem. A 1 (2013) 8805–8812.
[44] P. Zhou, D. Dang, M. Xiao, Q. Wang, J. Zhong, H. Tan, Y. Pei, R. Yang, W. Zhu, J. Mater. Chem. A (2015), http://dx.doi.org/10.1039/C5TA00166H.
[45] Y. Zhang, M. Xiao, N. Su, J. Zhong, H. Tan, Y. Wang, Y. Liu, Y. Pei, R. Yang, W. Zhu, Org. Electron. 17 (2015) 198–207.
[46] D. Demeter, T. Rousseau, P. Leriche, T. Cauchy, R. Po, J. Roncali, Adv. Funct. Mater. 21 (2011) 4379–4387.
[47] W. Li, Q. Li, C. Duan, S. Liu, L. Ying, F. Huang, Y. Cao, Dyes Pigments 113 (2015) 1–7.
[48] S.-C. Lan, P. Raghunath, Y.-H. Lu, Y.-C. Wang, S.-W. Lin, C.-M. Liu, J.-M. Jiang, M.-C. Lin, K.-H. Wei, A.C.S. App, Mater. Inter. 6 (2014) 9298–9306.
[49] C.-Z. Li, C.-C. Chueh, H.-L. Yip, K.M. O'Malley, W.-C. Chen, A.K.Y. Jen, J. Mater. Chem. 22 (2012) 8574–8578.
[50] W. Ni, M. Li, X. Wan, H. Feng, B. Kan, Y. Zuo, Y. Chen, RSC Adv. 4 (2014) (1980). 31977-31980.
[51] C.W. Schlenker, M.E. Thompson, Chem. Commun. 47 (2011) 3702–3716.
[52] P.W.M. Blom, V.D. Mihailetchi, L.J.A. Koster, D.E. Markov, Adv. Mater. 19 (2007) 1551–1566.
[53] L. Lu, Z. Luo, T. Xu, L. Yu, Nano Lett. 13 (2012) 59–64.
[54] Z. He, C. Zhong, S. Su, M. Xu, H. Wu, Y. Cao, Nat. Photon 6 (2012) 591–595.
[55] Z. He, C. Zhong, X. Huang, W.-Y. Wong, H. Wu, L. Chen, S. Su, Y. Cao, Adv. Mater. 23 (2011) 4636–4643.
[56] Q. Zhang, B. Kan, F. Liu, G. Long, X. Wan, X. Chen, Y. Zuo, W. Ni, H. Zhang, M. Li, Z. Hu, F. Huang, Y. Cao, Z. Liang, M. Zhang, T.P. Russell, Y. Chen, Nat. Photon 9 (2015) 35–41.
[57] G. Garcia-Belmonte, A. Munar, E.M. Barea, J. Bisquert, I. Ugarte, R. Pacios, Org. Electron. 9 (2008) 847–851.
[58] C.M. Proctor, M. Kuik, T.-Q. Nguyen, Prog. Polym. Sci. 38 (2013) 1941–1960.
[59] X. Yang, J. Loos, S.C. Veenstra, W.J.H. Verhees, M.M. Wienk, J.M. Kroon, M.A.J. Michels, R.A.J. Janssen, Nano Lett. 5 (2005) 579–583.